Earth and Planetary Science Letters 391 (2014) 288–295

Contents lists available at ScienceDirect

Earth and Planetary Science Letters

www.elsevier.com/locate/epsl

Contrasting sound velocity and intermediate-range structural order between polymerized and depolymerized silicate glasses under pressure

Tatsuya Sakamaki [a,b,*], Yoshio Kono [c], Yanbin Wang [a], Changyong Park [c], Tony Yu [a], Zhicheng Jing [a,d], Guoyin Shen [c]

[a] GeoSoilEnviroCARS, Center for Advanced Radiation Sources, The University of Chicago, Chicago, IL 60637, USA
[b] Department of Earth and Planetary Materials Science, Tohoku University, Sendai 980-8578, Japan [1]
[c] HPCAT, Geophysical Laboratory, Carnegie Institution of Washington, Argonne, IL 60439, USA
[d] Department of Earth, Environmental, and Planetary Sciences, Case Western Reserve University, Cleveland, OH 44106, USA [1]

ARTICLE INFO

Article history:
Received 28 January 2013
Received in revised form 6 January 2014
Accepted 3 February 2014
Available online 21 February 2014
Editor: C. Sotin

Keywords:
silicate glass
sound velocity
structure
degree of polymerization

ABSTRACT

X-ray diffraction and ultrasonic velocity measurements of three silicate glasses (in jadeite, albite, and diopside compositions) show a sharp contrast in pressure-induced changes in structure and elasticity. With increasing pressure to around 6 GPa, polymerized glasses (jadeite and albite) display large shift in the first sharp diffraction peak (FSDP) in the structure factor, $S(Q)$, to higher-Q values, indicating rapid shrinkage in the intermediate-range ordered (IRO) structure. Above 6 GPa, the shift of FSDP decelerates, suggesting that shrinkage in the IRO structure has been largely completed and the structure evolution is now dominated by the diminution of the interstitial volume in a more densely packed arrangement. Associated with this structural change, sound velocities increase with pressure above 6 GPa. In contrast, the depolymerized diopside glass exhibits smaller changes in the pressure dependence for both sound velocities and FSDP positions. Compared to the polymerized glasses, the velocities are faster and the positions of FSDP appear at higher-Q under the same experimental conditions. The results suggest that the depolymerized diopside glass has an initially denser IRO structure compared to that of the polymerized glasses, and there are no sufficient interstitial voids to shrink. The different behaviors between polymerized and depolymerized glasses are apparently related to the initial linkage of tetrahedra and the pressure-induced structural reactions. These results suggest that under compression up to 10 GPa, the degree of polymerization is a major factor affecting the IRO network structure and the sound velocity of silicate glasses.

© 2014 Elsevier B.V. All rights reserved.

1. Introduction

Igneous activities are primarily controlled by magmas, which occur in various geological/geophysical settings and have a wide range of compositions (e.g., basalt–andesite–rhyolite). These compositional differences largely determine structures of the magmas at depths and fundamentally control magma properties, which, in turn, control variations in eruption styles (e.g., Eichelberger et al., 1986). One of the most important parameters for constraining magma behaviors in the interior of the Earth is the degree of polymerization. Under upper mantle conditions, this is a useful indicator for the connectivity of SiO_2 tetrahedra, which are the basic units in all silicate melts. Compositional differences are generally considered in terms of variety of alkaline (e.g., Na^+) and alkaline–earth (e.g., Mg^{2+}, Ca^{2+}) cations in the melts. These cations, called network modifiers, tend to cut Si–O–Si bonds between adjacent SiO_4 tetrahedra (e.g., Mysen et al., 1982). Al^{3+} behaves as an intermediate species in silicate melts; it can act as either a network former (on the tetrahedral site) or a modifier, depending on composition (e.g., Riebling, 1966; Mysen et al., 1981). In the case of a fully-polymerized melt, such as jadeite and albite, all TO_4 tetrahedra are interconnected via oxygen anions, forming a continuous three-dimensional network. Whereas, for depolymerized diopside melt, approximately half the tetrahedral corners are disconnected. It is likely that the difference in the degree of polymerization results in different structural responses and physical properties of silicate melts.

* Corresponding author at: Department of Earth and Planetary Materials Science, Tohoku University, Sendai 980-8578, Japan. Tel.: +81 22 795 6666; fax: +81 22 795 6666.
E-mail address: sakamaki@m.tohoku.ac.jp (T. Sakamaki).
[1] Present address.

http://dx.doi.org/10.1016/j.epsl.2014.02.008
0012-821X/© 2014 Elsevier B.V. All rights reserved.

Because of the technical difficulties in measuring structure and properties of silicate melts under high pressure and high temperature conditions, many researchers instead have made efforts for obtaining insights by studying glasses which are quenched from melts. The relationship between the degree of polymerization and the structure/properties of quenched (or supercooled) silicate melts under pressure has been reported previously (e.g., Allwardt et al., 2004, 2005, 2007; Lee, 2004, 2011; Lee et al., 2003, 2004, 2006, 2012; Xue et al., 1989, 1991). In addition to the quenched silicate glass studies at ambient condition, in-situ high-pressure structure and/or property measurements on silicate glasses have also been conducted. For example, silica glass (SiO_2) has been well studied for pressure-induced changes in structure, density, and elastic properties (Susman et al., 1991; Meade et al., 1992; Zha et al., 1994; Sugai and Onodera, 1996; Tsiok et al., 1998; Clark et al., 2004; Inamura et al., 2004; Sato and Funamori, 2008, 2010; Murakami and Bass, 2010; Yokoyama et al., 2010; Kono et al., 2011). Sound velocities of SiO_2 glass up to 57.5 GPa have been investigated using the Brillouin scattering measurement (Zha et al., 1994). In this latter study, a negative pressure dependence in velocities up to about 3 GPa is reported, followed by a drastic increase in the velocities between 12 and 23 GPa. Ultrasonic velocity measurements have also been performed on SiO_2 glass (Yokoyama et al., 2010; Kono et al., 2011). In both studies, anomalous minima in V_P and V_S around 3 GPa were also found, confirming the Brillouin scattering measurements.

However, the effect of degree of polymerization in silicate melts/glasses on the structural response and physical properties under high pressure remains unclear (e.g., effect of degree of polymerization on the IRO, sound velocity, density, as well as pressure dependence of these properties). For silicate melts at ambient pressure, the degree of polymerization is closely related to composition and is quantitatively described by a ratio of non-bridging oxygens (NBO) to tetrahedral cations (T) (NBO/T; Mysen et al., 1982). The NBO/T ratio is widely used in examining viscosity systematics in various silicate melts and discussing magma mobility in the Earth's interior (e.g., Suzuki et al., 2005). Experimental data show that polymerized melts generally possess much higher values of viscosity than those of depolymerized ones near 1 atm (Dingwell and Virgo, 1988; Richet et al., 1996; Dingwell et al., 2004) and that pressure dependences of the viscosities for polymerized and depolymerized melts are fundamentally different: while viscosities of polymerized melts decrease with increasing pressure, those of depolymerized melts increase (Taniguchi, 1992; Wolf and McMillan, 1995; Poe et al., 1997; Funakoshi et al., 2002; Reid et al., 2003; Liebske et al., 2005; Suzuki et al., 2005, 2011; Lesher, 2010; Sakamaki et al., 2013). Although NBO fraction in the silicate glass generally decreases gradually with pressure (e.g., Lee, 2011), NBO/T under ambient condition appears to be a useful indicator for understanding the behavior of silicate melts.

In this study, we investigate sound velocities of polymerized (jadeite and albite composition: NBO/T = 0 at 1 atm) and depolymerized (diopside composition: NBO/T = 2 at 1 atm) glasses at pressures up to 10 GPa by using ultrasonic technique and synchrotron X-ray imaging in a Paris–Edinburgh press. We also study X-ray structure factors, $S(Q)$, of these glasses by using the multi-angle energy-dispersive X-ray diffraction technique, in order to understand structural changes in the intermediate-range order (IRO) with pressure. Finally, we discuss the correlation between sound velocities and structures, and the influence of the degree of polymerization on these properties.

2. Experimental methods

All experiments were conducted in a Paris–Edinburgh press, installed at the HPCAT 16-BM-B beamline, Advanced Photon Source (APS). Details of the setup are given by Kono et al. (2013). A schematic illustration of the high-pressure cell assembly is shown in Fig. 1. The outer pressure media consisted of machinable zirconia pallets and sintered boron-epoxy. Graphite cylinder was used as a sample container, with a gold foil placed on top and bottom of the capsule as markers for sample length measurements.

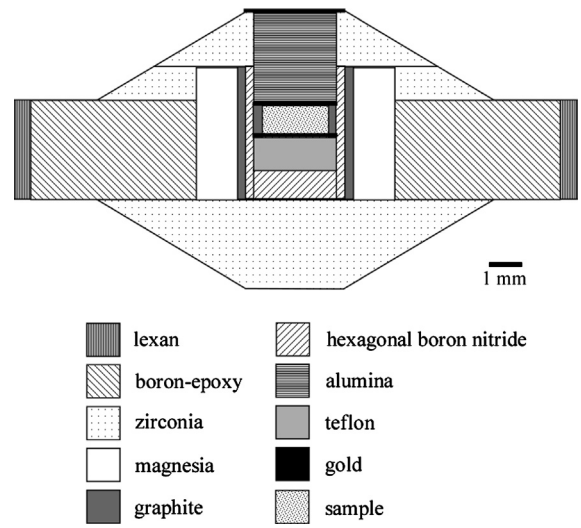

Fig. 1. A design of cell assembly for ultrasonic measurements.

X-ray radiography images allowed us to determine sample lengths under high pressure (Fig. 2a). A fully densified alumina cylinder above the sample was used as a buffer rod for the transmission of ultrasonic signals. Both the glass sample and the alumina buffer rod were polished with 1 μm diamond paste to ensure good mechanical contact. High-pressure sound velocity measurements were carried out using the ultrasonic pulse-echo-overlap method. Details of the ultrasonic measurement are described in Kono et al. (2012). Ultrasonic signals were generated and received by a $LiNbO_3$ transducer. The signals were collected with a sampling rate of 5×10^9 Hz (Fig. 2b). The compressional and shear wave travel times were determined using the reflected signals from the buffer rod/sample (R1) and sample/teflon (R2) interfaces. The travel time was determined within the uncertainty of ±0.1 ns, corresponding to an uncertainty in compressional and shear wave velocities of up to ±0.08% and ±0.05%, respectively. Uncertainty of the sample length determination was less than ±0.948 μm (±1 pixel) in a conservative estimation, because the buffer rod/sample and sample/backing reflector interface position was determined with the standard deviation of less than ±0.190 μm (±0.2 pixel), respectively. The ±0.948 μm uncertainty in sample length determination corresponds to ±0.26% error in both compressional- and shear-wave velocity determinations. We therefore consider the overall uncertainty in the compressional and shear wave velocity measurement to be less than ±0.34% and ±0.30%, respectively.

Structure measurements were performed using the energy dispersive X-ray diffraction (XRD) technique as described in Yamada et al. (2011). The 16-BM-B is a bending magnet beamline providing white X-rays (5–120 keV) with high brightness. The incident X-ray beam was collimated by two sets of vertical (0.1 mm) and horizontal (0.1 mm) slits. The diffracted signal was collimated with a 0.1 mm gap collimator, 60 mm downstream from the sample, and a 0.1 mm (H) × 5.0 mm (V) receiving slit 480 mm further downstream from the scattering slits. A Ge-SSD with a 4096 multi-channel analyzer was mounted on a two-theta arm, on air pads over a granite table, on a large Huber rotation stage, which allowed accurate control of the two-theta angles. Diffraction patterns were collected at 9 fixed diffraction angles ($2\theta = 3°, 4°, 5°, 7°, 9°, 11°, 15°, 20°, 25°$). Collecting time varied with

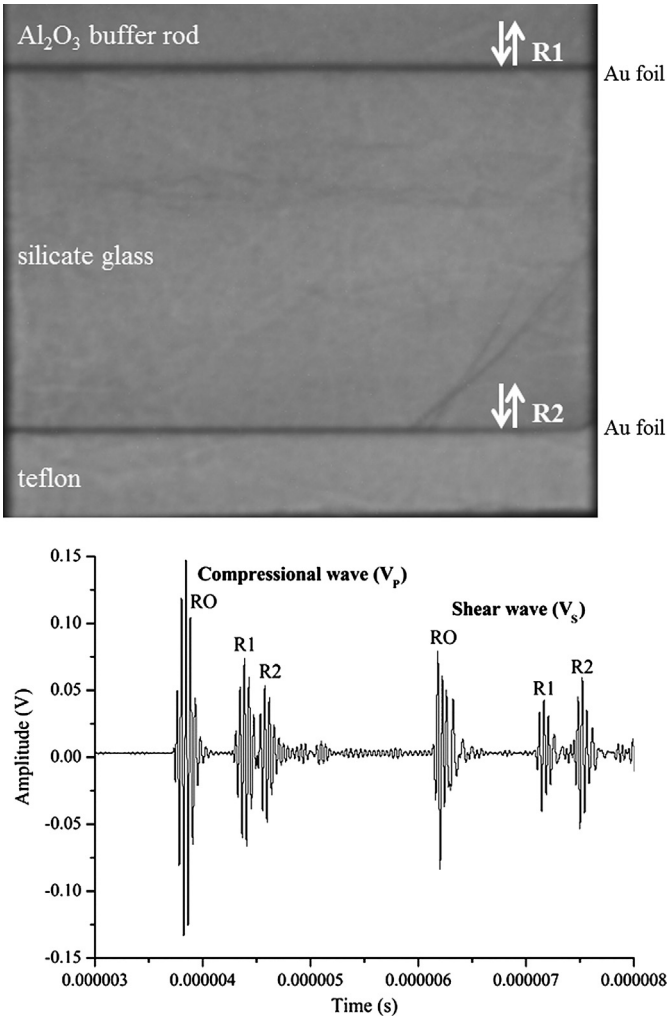

Fig. 2. (a) An example of X-ray radiography image of sample (diopside glass) at 1.2 GPa. (b) An example of compressional and shear wave signals reflected at anvil/Al_2O_3 buffer rod (R0), Al_2O_3 buffer rod/diopside glass (R1), and diopside glass/teflon (R2) interfaces at pressure of 1.2 GPa.

diffraction angles as intensities decreased with increasing angle. All patterns were collected until the maximum intensity reached at least 2000 counts. Structure factors, $S(Q)$s, were obtained from the measured X-ray diffraction data using the analytical program by Funakoshi (1997).

Pressure was determined by the equation of state of gold (Tsuchiya, 2003), of which the diffraction patters were collected from the foil below the sample.

3. Results

3.1. Sound velocities under pressure

Experimental results are summarized in Table 1. The difference in sound velocities at ambient pressure between polymerized and depolymerized glasses/melts is partly due to the difference in chemical compositions (e.g., Rivers and Carmichael, 1987). Pressure dependence of both compressional wave velocity, V_P, and shear wave velocity, V_S, are shown in Figs. 3a and 3b, respectively. Velocities of silica (Zha et al., 1994), a polymerized glass (NBO/T = 0 at 1 atm), and enstatite (Sanchez-Valle and Bass, 2010), a depolymerized glass (NBO/T = 2 at 1 atm), are also plotted for comparison. Two pressure regions with marked changes in the pressure dependence of sound velocities are identified in polymerized

Table 1
Experimental result of sound velocity measurements. Uncertainties in calculated densities at high pressure are less than 1%.

Pressure (GPa)	V_P (km/s)	V_S (km/s)	V_B (km/s)	Poisson's ratio	Density (g/cm^3)
Jadeite					
0.0					2.531 (8)
0.9	5.466 (19)	3.292 (10)	3.928 (15)	0.215 (1)	2.586
1.4	5.464 (19)	3.255 (10)	3.965 (15)	0.225 (1)	2.617
2.2	5.417 (18)	3.226 (10)	3.934 (15)	0.225 (1)	2.670
2.8	5.349 (18)	3.186 (10)	3.883 (15)	0.225 (1)	2.709
3.0	5.350 (18)	3.193 (10)	3.876 (15)	0.223 (1)	2.724
3.0	5.323 (18)	3.173 (10)	3.862 (15)	0.224 (1)	2.725
3.4	5.272 (18)	3.160 (9)	3.805 (14)	0.220 (1)	2.755
3.5	5.258 (18)	3.133 (9)	3.816 (14)	0.225 (1)	2.761
4.1	5.272 (18)	3.118 (9)	3.851 (14)	0.231 (1)	2.800
4.4	5.241 (18)	3.111 (9)	3.816 (14)	0.228 (1)	2.819
4.5	5.279 (18)	3.095 (9)	3.885 (14)	0.238 (1)	2.829
4.6	5.250 (18)	3.099 (9)	3.841 (14)	0.233 (1)	2.837
5.1	5.225 (18)	3.061 (9)	3.849 (14)	0.239 (1)	2.868
5.3	5.227 (18)	3.052 (9)	3.861 (14)	0.241 (1)	2.884
5.6	5.210 (18)	3.048 (9)	3.841 (15)	0.240 (1)	2.901
6.1	5.230 (18)	3.031 (9)	3.887 (14)	0.247 (1)	2.933
6.2	5.275 (18)	3.028 (9)	3.949 (15)	0.254 (1)	2.940
6.6	5.317 (18)	3.044 (9)	3.990 (15)	0.256 (1)	2.969
7.0	5.315 (18)	3.036 (9)	3.995 (14)	0.258 (1)	2.991
7.0	5.313 (18)	3.026 (9)	4.003 (15)	0.260 (1)	2.992
7.3	5.352 (18)	3.019 (9)	4.061 (15)	0.267 (1)	3.007
7.3	5.380 (18)	3.026 (9)	4.091 (15)	0.269 (1)	3.009
7.5	5.439 (18)	3.048 (9)	4.147 (15)	0.271 (1)	3.023
7.6	5.472 (19)	3.047 (9)	4.191 (15)	0.275 (1)	3.029
7.9	5.518 (19)	3.054 (9)	4.245 (16)	0.279 (1)	3.045
8.3	5.550 (19)	3.057 (9)	4.282 (16)	0.282 (1)	3.064
8.3	5.691 (19)	3.099 (9)	4.425 (16)	0.289 (1)	3.064
8.8	5.777 (20)	3.101 (9)	4.533 (17)	0.298 (1)	3.089
9.1	5.854 (20)	3.150 (9)	4.587 (17)	0.296 (1)	3.103
9.6	5.877 (20)	3.160 (9)	4.607 (17)	0.297 (1)	3.130
Albite					
0.0					2.460 (7)
1.4	5.571 (19)	3.469 (10)	3.871 (15)	0.183 (1)	2.556
1.3	5.468 (19)	3.370 (10)	3.841 (15)	0.194 (1)	2.544
2.0	5.381 (18)	3.317 (10)	3.779 (14)	0.194 (1)	2.596
2.8	5.306 (18)	3.249 (10)	3.753 (14)	0.200 (1)	2.653
3.6	5.250 (18)	3.205 (10)	3.723 (14)	0.203 (1)	2.709
3.8	5.196 (18)	3.179 (10)	3.678 (14)	0.201 (1)	2.726
4.8	5.184 (18)	3.146 (9)	3.699 (14)	0.209 (1)	2.800
4.6	5.167 (18)	3.119 (9)	3.705 (14)	0.213 (1)	2.783
4.5	5.174 (18)	3.105 (9)	3.730 (14)	0.219 (1)	2.779
4.8	5.176 (18)	3.120 (9)	3.717 (14)	0.215 (1)	2.801
5.8	5.204 (18)	3.090 (9)	3.788 (14)	0.228 (1)	2.866
5.8	5.185 (18)	3.100 (9)	3.751 (14)	0.222 (1)	2.869
6.1	5.224 (18)	3.107 (9)	3.797 (14)	0.226 (1)	2.890
6.5	5.252 (18)	3.082 (9)	3.863 (14)	0.237 (1)	2.919
6.9	5.286 (18)	3.117 (9)	3.871 (14)	0.233 (1)	2.945
7.1	5.341 (18)	3.123 (9)	3.939 (15)	0.240 (1)	2.954
7.4	5.388 (18)	3.117 (9)	4.010 (15)	0.249 (1)	2.975
Diopside					
0.0					2.920 (13)
0.8	6.667 (23)	3.636 (11)	5.179 (19)	0.288 (1)	2.951
1.0	6.696 (23)	3.589 (11)	5.260 (19)	0.298 (1)	2.959
1.2	6.718 (23)	3.585 (11)	5.290 (19)	0.301 (1)	2.964
1.9	6.733 (23)	3.586 (11)	5.310 (19)	0.302 (1)	2.989
1.8	6.748 (23)	3.587 (11)	5.327 (19)	0.303 (1)	2.987
2.1	6.770 (23)	3.594 (11)	5.349 (19)	0.304 (1)	2.995
2.2	6.792 (23)	3.590 (11)	5.380 (20)	0.306 (1)	2.998
3.3	6.807 (23)	3.611 (11)	5.380 (20)	0.304 (1)	3.037
2.1	6.816 (23)	3.618 (11)	5.386 (20)	0.304 (1)	2.995
3.4	6.828 (23)	3.620 (11)	5.399 (20)	0.304 (1)	3.041
3.5	6.851 (23)	3.620 (11)	5.428 (20)	0.306 (1)	3.044
3.8	6.871 (23)	3.616 (11)	5.457 (20)	0.309 (1)	3.056
3.7	6.886 (23)	3.615 (11)	5.476 (20)	0.310 (1)	3.052
4.6	6.857 (23)	3.596 (11)	5.457 (20)	0.310 (1)	3.082
6.2	6.870 (23)	3.577 (11)	5.490 (20)	0.314 (1)	3.133
6.2	6.875 (23)	3.562 (11)	5.507 (20)	0.316 (1)	3.133
6.5	6.867 (23)	3.561 (11)	5.500 (20)	0.316 (1)	3.144
7.1	6.862 (23)	3.546 (11)	5.506 (20)	0.318 (1)	3.164
8.4	6.852 (23)	3.550 (11)	5.491 (20)	0.317 (1)	3.207

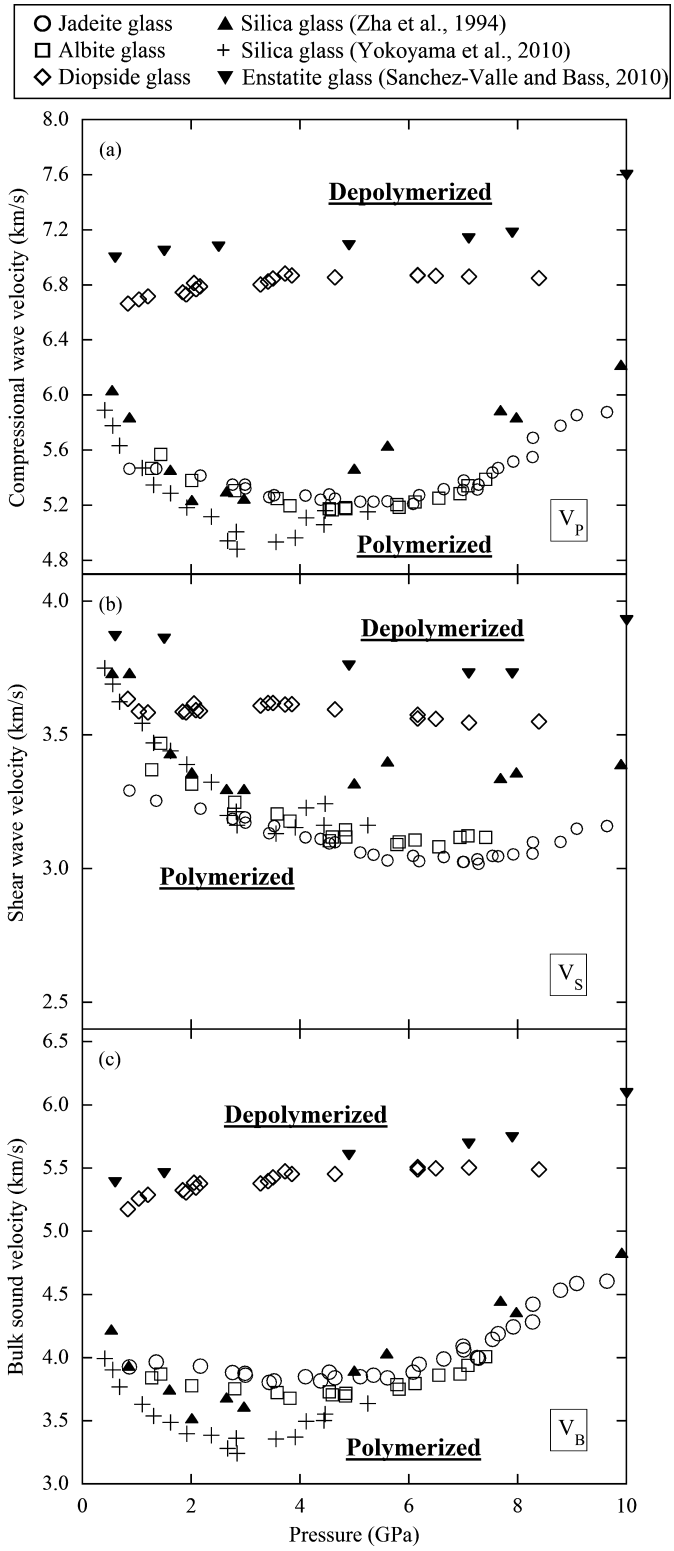

Fig. 3. Compressional wave velocities (a), shear wave velocities (b), and bulk sound velocities (c) of silicate glasses as a function of pressure. The data of silica and enstatite glass are from Zha et al. (1994) and Sanchez-Valle and Bass (2010), respectively. Jadeite, albite and silica glass are polymerized glasses (NBO/T = 0) and diopside and enstatite glasses are depolymerized glasses (NBO/T = 2). Error bars are smaller than symbols.

(jadeite and albite) glasses. Below 6 GPa, sound velocities exhibit negative pressure dependence; above 6 GPa, velocities increase rapidly with pressure. The pressure dependences of velocities of these polymerized glasses show similar trend to that of silica glass (Zha et al., 1994). The marked difference in pressure dependence of sound velocities suggests a change in compression mechanism. In the case of depolymerized (diopside) glass, no obvious change in the pressure dependence of sound velocities is observed; both V_P and V_S are higher than those of jadeite and albite glasses. Magnitude of the pressure dependence in diopside glass is also smaller than those of jadeite and albite glasses.

Using the compressional and shear velocities, bulk sound velocities (V_B) are calculated using the following equation,

$$V_B = \sqrt{V_P^2 - \frac{4}{3}V_S^2} = \sqrt{\frac{K_S}{\rho}}, \quad (1)$$

where K_S is the adiabatic bulk modulus and ρ is density. The pressure dependence of V_B also clearly falls into two groups (Fig. 3c), one for polymerized (jadeite, albite, and silica) glasses, and the other for depolymerized (diopside and enstatite) glasses. The results show that the degree of polymerization is fundamentally related to the compression behavior of silicate glasses.

The observed pressure dependence of velocities is summarized as follows (Table 2). For jadeite and albite glasses, V_B is nearly constant up to 6 GPa and then increases rapidly, while V_S decreases slowly up to 6 GPa and remains relatively constant with very little increase after that. For diopside glass, V_S is nearly constant up to about 4 GPa and decreases after that, but V_B increases up to about 4 GPa and remains nearly constant after that. V_P, on the other hand, reaches a maximum at ∼4 GPa. The sequence of velocity variation in diopside glass is essentially reversed compared with jadeite and albite glasses. Furthermore, the slopes are very different and the turn-over pressure point is ∼6 GPa for jadeite and albite glasses, ∼4 GPa for diopside.

3.2. Structural responses to pressure

Fig. 4 shows results of structural evolution. Structure factors $S(Q)$ of jadeite glass up to 9.6 GPa are shown in Fig. 4a. The first sharp diffraction peak (FSDP), typically centered around 1–3 Å^{-1} in $S(Q)$ for silicates, is in general a signature of the ···–T–O–T–··· IRO in silicate network (e.g., Elliott, 1991). Peaks at lower-Qs in reciprocal space reflect longer range ordering in real space. The positive pressure dependence of the FSDP in Q-space in jadeite glass represents a rapid decrease in the intermediate correlation distances in real space with pressure. Shrinkage of IRO corresponds to the change of TO_4 configuration in the network, such as a decrease in ···–T–O–T–··· bond angles of tetrahedron and the reduction of void space in the network. For jadeite glass, FSDP moves towards higher-Q monotonically with increasing pressure up to 7.4 GPa, suggesting continuous shrinkage of the network structure, by changing the intermediate-range ordering, such as reducing –T–O–T– angle. Between 7.4 and 9.6 GPa, the FSDP position moves more slowly than the lower pressure region. The sharp change in the slope suggests again a change in compression mechanism around this pressure.

In addition to the large shift to higher-Q in the FSDP position, $S(Q)$ provides additional evidence of densification of the jadeite glass. Above 7.4 GPa, a small peak appears on the right side (∼3.0–3.2 Å^{-1}) of the FSDPs in $S(Q)$, termed "second sharp diffraction peak (SSDP)" by Elliott (1995). The SSDP, which denotes a diminution of the interstitial volume between the silicate network (Salmon et al., 2005, 2006), has been reported in previous X-ray diffraction studies on silicate glasses and melts (e.g., Meade et al., 1992; Inamura et al., 2004; Yamada et al., 2011) attributed to more densely packed structure.

Structure factors of albite glass are shown in Fig. 4b. Similar to jadeite glass, the FSDP position in albite also shifts rapidly to

Table 2
Summary of the pressure dependence of sound velocities in silicate glasses.

Silicate glass	V_P	V_S	V_B
Jadeite/Albite (NBO/T = 0 at 1 atm)	Minimum at ∼6 GPa (↘↗)	decrease below 4 GPa (↘) constant above 4 GPa (→)	constant below 4 GPa (→) increase above 4 GPa (↗)
Diopside (NBO/T = 2 at 1 atm)	Maximum at ∼4 GPa (↗↘)	constant below 4 GPa (→) decrease above 4 GPa (↘)	constant below 4 GPa (→) increase above 4 GPa (↗)

higher-Q between 1 atm and 5.5 GPa, suggesting significant densification, and slows down above 5.5 GPa. This change in pressure dependence also corresponds to the appearance of SSDP above 7.3 GPa, as is observed in jadeite glass.

In contrast, diopside glass shows a rather different compression behavior in structure factors as shown in Fig. 4c. The positions of FSDP are located at higher-Q values and show little change with increasing pressure.

4. Discussion

4.1. Contrasting compression mechanisms of polymerized versus depolymerized glasses

In this study, the most pronounced difference in $S(Q)$ between polymerized and depolymerized glasses is the positions of FSDP and its pressure dependence (Fig. 5). The FSDP of diopside glass at ambient pressure appears at higher-Q than those of jadeite and albite glasses, meaning that diopside glass has a more packed IRO structure than the jadeite and albite counterparts. More importantly, the pressure dependence of FSDP in diopside glass is significantly smaller compared to those in jadeite and albite glasses. In addition, the peak shifts of diopside glass are more likely monotonic with pressure. This also suggests that diopside glass possesses fewer interstitial voids to accommodate pressure-induced modification in the IRO.

These differences in IRO structure are well consistent with the observations in bulk sound velocities (Fig. 3c): bulk sound velocities of diopside glass are significantly higher than those of jadeite and albite glasses, and its pressure dependence increases slightly with increasing pressure. In fully polymerized tetrahedral glasses such as silica and Germania (SiO_2 and GeO_2, NBO/T = 0), the structural response to pressure is dominated by the tightening of the T–O–T bond angle (e.g., Susman et al., 1991; Salmon et al., 2012). Since each T cation is statistically connected to four adjacent T cations, the bending of the T–O–T bond angle results in an overall volume response to pressure. Thus silica exhibits a "softening" in both bulk and shear moduli upon compression (e.g., Kono et al., 2012). According to the rigidity percolation theory (Thorpe, 1983) 2.4 connections are required between each structural unit to form a fully continuous 3D network. For tetrahedral random networks, this means that when NBO/T $\geqslant$ 1.6, there are too few tetrahedron–tetrahedron connections to form fully continuous 3D networks (Phillips, 1979). Unlike chalcogenide systems, here percolation (or rigidity) is applied to inter-tetrahedral bonds instead of inter-atomic bonds, as TO_4 are considered to act like fixed units in silicate liquids.

For jadeite glass, the presence of Na^+ cations helps Al^{3+} build tetrahedral network along with Si^{4+} while maintaining charge balance, whereas Mg^{2+} and Ca^{2+} cations in diopside glass play a role as network modifiers (i.e., network breakers). The initial structural changes in response to compression are therefore different: for polymerized jadeite glass is most likely the T–O–T angle reduction (as has been observed in jadeite melt by Wang et al., 2014), whereas for depolymerized diopside glass and melt, it is the reduction of Mg–O and Ca–O bond-lengths. Our observations are consistent with these compression mechanisms and show that structural responses are the key in explaining the pressure dependence in elastic properties and density of glasses.

4.2. Difference in properties between polymerized and depolymerized glasses

4.2.1. Sound velocity and Poisson's ratio

Sound velocity measurements support the notion of two different structural compression mechanisms below and above about 6 GPa in polymerized glasses, as the pressure regions of observed structural changes are consistent with those in sound velocity measurements. In the low-pressure region (<6 GPa), drastic shrinkage of IRO network of polymerized glasses occurs, causing an abnormal decrease in the sound velocities. Around 6 GPa, major densification appears to have completed with no significant interstitial voids left in the glass. Hence in the high-pressure region (>6 GPa), structural shrinkage diminishes, and the velocities begin to increase with pressure. In the case of depolymerized glass, there are no drastic changes in structure and sound velocities up to about 8 GPa, the maximum pressure of this study for diopside glass. Effects of Mg and Ca on the observed behavior of V_P and V_S appear less important under pressure, because the results of enstatite and diopside show similar behavior. If the difference in the pressure dependence of V_P and V_S is due to Mg and Ca, there should be clear trend among $NaAlSi_2O_6$ Jadeite (Mg = 0, Ca = 0), $CaMgSi_2O_6$ diopside (Mg = 1, Ca = 1), and $Mg_2Si_2O_6$ enstatite (Mg = 2, Ca = 0). Thus, we conclude that the degree of polymerization has a profound influence on the correlation between sound velocities and IRO structure.

The Poisson's ratio (σ) is obtained directly from the measured sound velocities by,

$$\sigma = \frac{V_P^2 - 2V_S^2}{2(V_P^2 - V_S^2)} \tag{2}$$

and its pressure dependence is shown in Fig. 6. In the case of depolymerized glasses, the Poisson's ratio is about 0.30 at ambient pressure and seems to increase nearly linearly with pressure. On the other hand, polymerized glasses generally have lower Poisson's ratios (between 0.15 and 0.22) at ambient condition, with significantly higher pressure dependence, especially above 5–6 GPa.

Poisson's ratio, which measures a material's resistance to distort under mechanical load, is affected by atomic arrangements in silicate glasses (Greaves et al., 2011). For polymerized jadeite and albite glasses (NBO/T = 0), the continuous three-dimensional (3D) tetrahedral network imposes structural constraints on how the glasses respond to mechanical stress. Especially, the tightening of the T–O–T angle in the 3D network may lead to low Poisson's ratios, analogous to recently discovered "metamaterials" (Babaee et al., 2013). On the other hand, depolymerized glasses, such as diopside and enstatite, are compressed via bond length reduction and tend to have higher Poisson's ratios. This is generally consistent with systematics over a large number of non-silicate glasses (Greaves et al., 2011).

4.2.2. Density

Assuming that all deformation is elastic, the density (ρ) of isotropic silicate glasses under pressure is calculated using the ambient density (ρ_0) through the relationship:

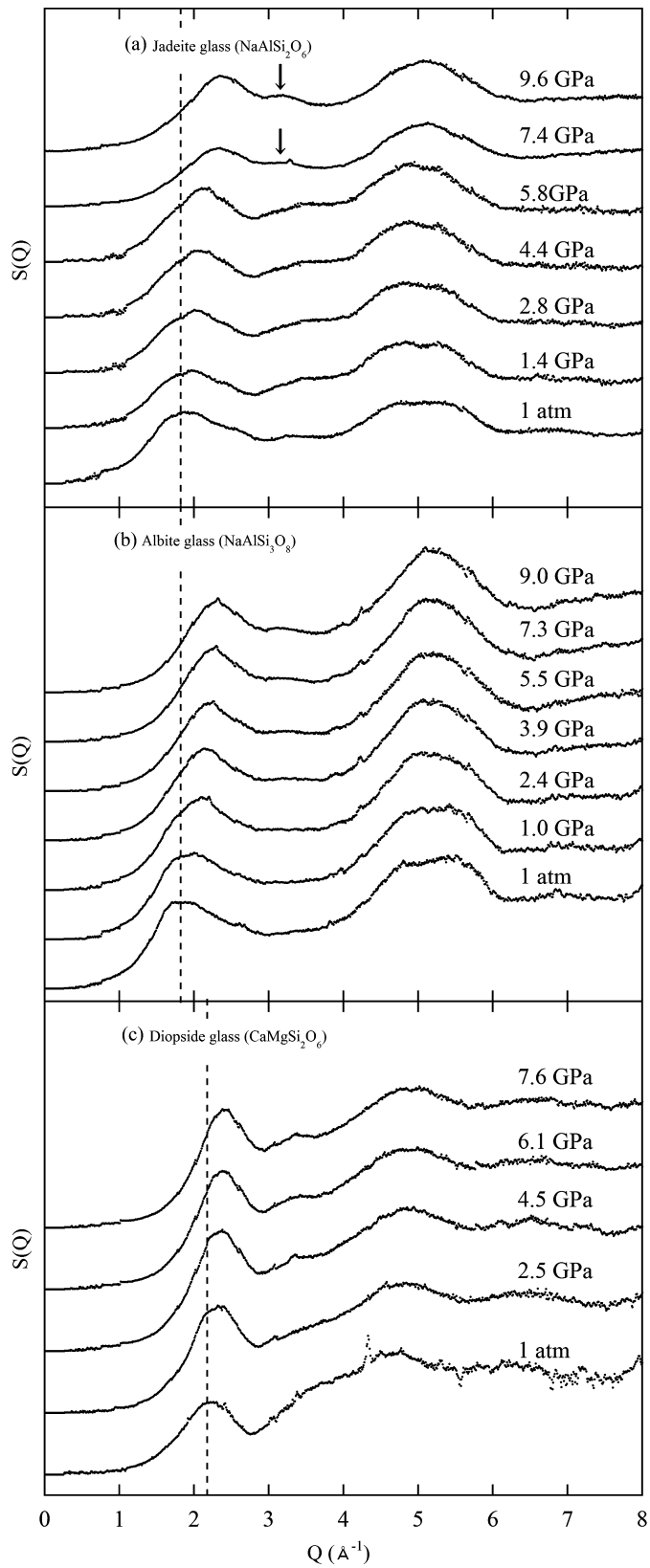

Fig. 4. Structure factors, $S(Q)$, of jadeite glass (a), albite glass (b), and diopside glass (c) with pressure. Vertical dotted lines indicate the FSDP position at 1 atm. Arrows in (a) indicate the SSDP.

$$\rho - \rho_0 = \int_{P_0}^{P} \gamma \frac{1}{V_B^2} dP. \quad (3)$$

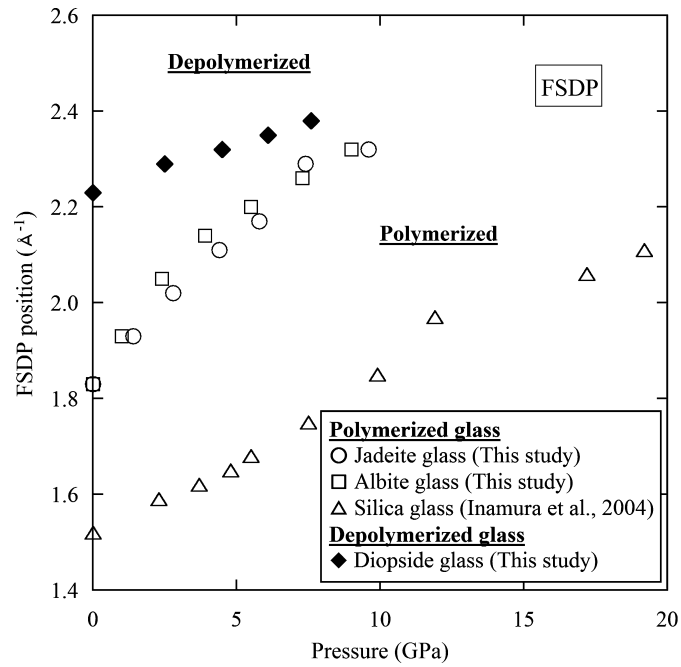

Fig. 5. FSDP positions of silicate glasses as a function of pressure. The data of silica glass is from Inamura et al. (2004). Jadeite, albite and silica glass are polymerized glasses (NBO/T = 0) and diopside glass is depolymerized glass (NBO/T = 2).

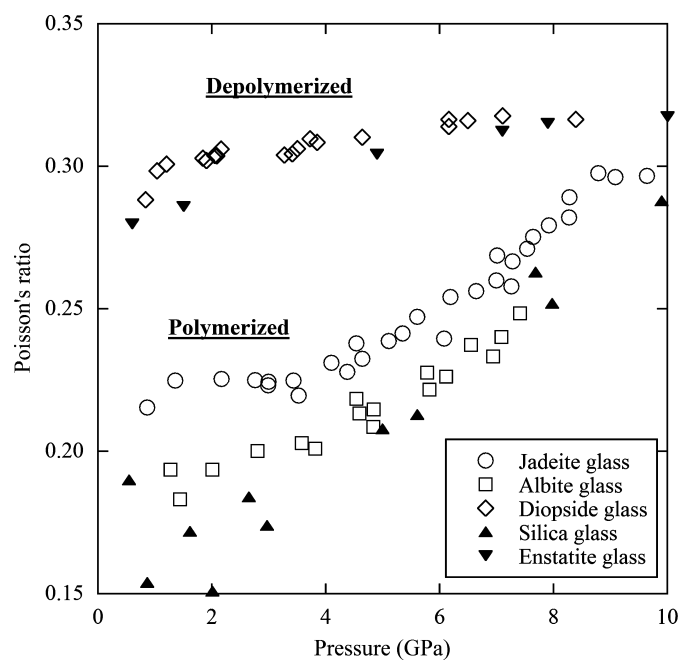

Fig. 6. Poisson's ratio of silicate glasses as a function of pressure. The data of silica and enstatite glass are from Zha et al. (1994) and Sanchez-Valle and Bass (2010), respectively. Jadeite, albite and silica glass are polymerized glasses (NBO/T = 0) and diopside and enstatite glasses are depolymerized glasses (NBO/T = 2). Error bars are smaller than symbols.

where γ is the ratio of the isothermal and adiabatic bulk moduli; γ is taken to be 1 for the present silicate glasses at ambient temperature. Densities of silicate glasses as a function of pressure are shown in Fig. 7a. The densities of silica glass (Zha et al., 1994) and enstatite glass (Sanchez-Valle and Bass, 2010) are also plotted for comparison. All densities increase monotonically with pressure. Densities of jadeite and albite glasses cross over that of enstatite

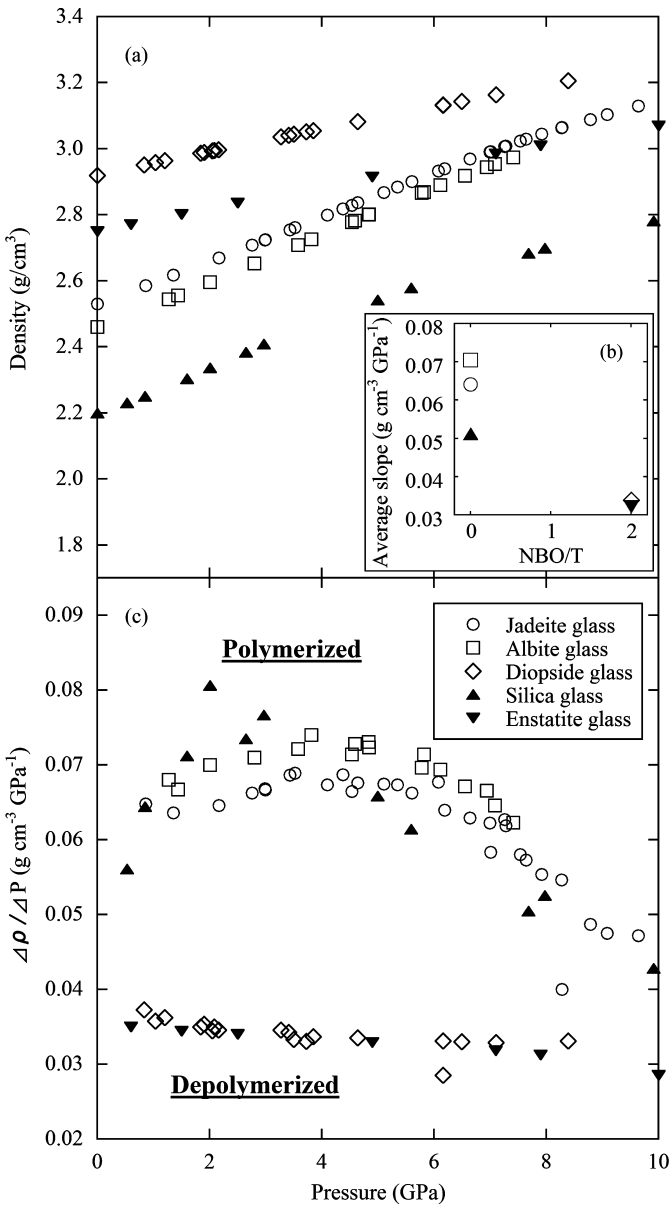

Fig. 7. (a) Density of silicate glasses as a function of pressure. The data of silica and enstatite glass are from Zha et al. (1994) and Sanchez-Valle and Bass (2010), respectively. Jadeite, albite and silica glass are polymerized glasses (NBO/T = 0) and diopside and enstatite glasses are depolymerized glasses (NBO/T = 2). Error bars are smaller than symbols. (b) The average slope of density-pressure diagram in silicate glasses as a function of NBO/T. The slope is calculated by linear fitting. (c) Pressure-dependence of density ($d\rho/dP$) of silicate glasses as a function of pressure.

around 8 GPa. Density crossover between diopside and jadeite/albite glasses may occur around 12 GPa.

However, there is a difference in compressibility between polymerized and depolymerized glasses. Fig. 7b indicates the average slopes, which are calculated by linear fitting of data in Fig. 7a as a function of NBO/T ratio. Diopside and enstatite glasses are denser than the others at ambient pressure, however their compressibility is lower and the density contrast between depolymerized and polymerized glasses becomes smaller at higher pressures.

Fig. 7c indicates the pressure-dependence of density ($d\rho/dP$) of silicate glasses. There is a systematic difference between polymerized and depolymerized glasses. The polymerized glasses show maxima in $d\rho/dP$ around 4 GPa. On the other hand, $d\rho/dP$ values of depolymerized glasses are much smaller, and decrease slightly with increasing pressure.

4.3. Implications to tectonics

Since the compression mechanisms of polymerized and depolymerized glasses observed here are similar to those of melts of the same compositions (Wang et al., 2014), our results on physical properties of compressed glasses may be applied to melts. According to Fig. 7 polymerized melts are denser and gravitationally more stable in the deep earth than depolymerized melts. Considering compositions of the Earth's component, melts with granitic continental crustal compositions are more polymerized than those of basaltic oceanic crust compositions. Recently, subduction of granitic materials by tectonic erosion, sediment-trapped subduction and direct subduction of immature oceanic arcs are indicated by geological and geophysical surveys (e.g., Plank and Langmuir, 1998; Jackson et al., 2007). The granitic melt generated at shallower depth is lighter and can return to the surface. However, if the granitic rock is transported to the deep mantle and melted under higher pressure conditions, the generated melt may be denser than surrounding mantle and gravitationally stable.

Acknowledgements

We thank Curtis Kenney-Benson (HPCAT) for his support during the experiments and Akio Suzuki (Tohoku Univ.) for the starting material. The experiments were performed at HPCAT Sector 16 at the Advanced Photon Source (APS), Argonne National Laboratory. HPCAT operations are supported by DOE-NNSA under Award No. DE-NA0001974 and DOE-BES under Award No. DE-FG02-99ER45775, with partial instrumentation funding by NSF. APS is supported by DOE-BES, under Contract No. DE-AC02-06CH11357. The PEP system was developed at GeoSoilEnviroCARS (Sector 13), APS. GeoSoilEnviroCARS is supported by the National Science Foundation Earth Sciences (EAR-0622171) and Department of Energy-Geosciences (DE-FG02-94ER14466). Y.W. and G.S. acknowledge the support from COMPRES and NSF Grants Nos. EAR 0711057, EAR 1214376 and EAR 0738852 for the development of this facility.

References

Allwardt, J.R., Schmidt, B.C., Stebbins, J.F., 2004. Structural mechanisms of compression and decompression in high pressure $K_2Si_4O_9$ glasses: An investigation utilizing Raman and NMR spectroscopy of high-pressure glasses and crystals. Chem. Geol. 213, 137–151.

Allwardt, J.R., Stebbins, J.F., Schmidt, B.C., Frost, D.J., Withers, A.C., Hirschmann, M.M., 2005. Aluminum coordination and the densification of high-pressure aluminosilicate glasses. Am. Mineral. 90, 1218–1222.

Allwardt, J.R., Stebbins, J.F., Terasaki, H., Du, L.S., Frost, D.J., Withers, A.C., Hirschmann, M.M., Suzuki, A., Ohtani, E., 2007. Effect of structural transitions on properties of high-pressure silicate melts: Al-27 NMR, glass densities, and melt viscosities. Am. Mineral. 92 (7), 1093–1104.

Babaee, S., Shim, J., Weaver, J.C., Chen, E.R., Patel, N., Bertoldi, K., 2013. 3D soft metamaterials with negative Poisson's ratio. Adv. Mater. 25, 5044–5049.

Clark, T.M., Grandinetti, P.J., Florian, P., Stebbins, J.F., 2004. Correlated structure distributions in silica glass. Phys. Rev. B 70, 064202.

Dingwell, D.B., Virgo, D., 1988. Viscosities of melts in the Na_2O–FeO–Fe_2O_3–SiO_2 system and factors controlling relative viscosities of fully polymerized silicate melts. Geochim. Cosmochim. Acta 52, 395–403.

Dingwell, D.B., Courtial, P., Giordano, D., Nichols, A.R.L., 2004. Viscosity of peridotite liquid. Earth Planet. Sci. Lett. 226, 127–138.

Eichelberger, J.C., Carrigan, C.R., Westrich, H.R., Price, R.H., 1986. Non-explosive silicic volcanism. Nature 323, 598–602.

Elliott, S.R., 1991. Medium-range structure order in covalent amorphous solids. Nature 354, 445–452.

Elliott, S.R., 1995. Second sharp diffraction peak in the structure factor of binary covalent network glasses. Phys. Rev. B 51, 8599–8601.

Funakoshi, K., 1997. Energy-dispersive x-ray diffraction for binary alkali silicate melts using synchrotron radiation under high pressure and temperature. Ph.D. dissertation. Tokyo Institute of Technology.

Funakoshi, K., Suzuki, A., Terasaki, H., 2002. In situ viscosity measurements of albite melt under high pressure. J. Phys. Condens. Matter 14, 11343–11347.

Greaves, G.N., Greer, A.L., Lakes, R.S., Rouxel, T., 2011. Poisson's ratio and modern materials. Nat. Mater. 10, 823–837.
Inamura, Y., Katayama, Y., Utsumi, W., Funakoshi, K., 2004. Transformations in the intermediate-range structure of SiO_2 glass under high pressure and temperature. Phys. Rev. Lett. 93, 015501.
Jackson, M.G., Hart, S.R., Koppers, A.A.P., Staudigel, H., Konter, J., Blusztajn, J., Kurz, M., Russell, J.A., 2007. The return of subducted continental crust in Samoan Lavas. Nature 448, 684–687.
Kono, Y., Yamada, A., Wang, Y., Yu, T., Inoue, T., 2011. Combined ultrasonic elastic wave velocity and microtomography measurements at high pressures. Rev. Sci. Instrum. 82, 023906.
Kono, Y., Park, C., Sakamaki, T., Kenny-Benson, C., Shen, G., Wang, Y., 2012. Simultaneous structure and elastic wave velocity measurement of SiO_2 glass at high pressures and high temperatures in a Paris–Edinburgh cell. Rev. Sci. Instrum. 83, 033905.
Kono, Y., Park, C., Kenney-Benson, C., Shen, G., Wang, Y., 2013. Toward comprehensive studies of liquids at high pressures and high temperatures: Combined structure, elastic wave velocity, and viscosity measurements in the Paris–Edinburgh cell. Phys. Earth Planet. Inter. http://dx.doi.org/10.1016/j.pepi.2013.09.006.
Lee, S.K., 2004. The structure of silicate melts at high pressure: Quantum chemical calculations and solid state NMR. J. Phys. Chem. B 108, 5889–5900.
Lee, S.K., 2011. Simplicity in melt densification in multi-component magmatic reservoirs in earth's interior revealed by multi-nuclear magnetic resonance. Proc. Natl. Acad. Sci. USA 108 (17), 6847–6852.
Lee, S.K., Fei, Y., Cody, G.D., Mysen, B.O., 2003. Order and disorder of sodium silicate glasses and melts at 10 GPa. Geophys. Res. Lett. 30, 1845.
Lee, S.K., Cody, G.D., Fei, Y., Mysen, B.O., 2004. The nature of polymerization and properties of silicate glasses and melts at high pressure. Geochim. Cosmochim. Acta 68, 4189–4200.
Lee, S.K., Cody, G.D., Fei, Y., Mysen, B.O., 2006. The effect of Na/Si on the structure of sodium silicate and aluminosilicate glasses quenched from melts at high pressure: A multi-nuclear (Al-27, Na-23, O-17) 1- and 2D solid-state NMR study. Chem. Geol. 229, 162–172.
Lee, S.K., Yi, Y.S., Cody, G.D., 2012. Effect of network polymerization on the pressure-induced structural changes in sodium aluminosilicate glasses and melts: Al-27 and O-17 solid-state NMR study. J. Phys. Chem. C 116, 2183–2191.
Lesher, C.E., 2010. Self-diffusion in silicate melts theory, observations and applications to magmatic systems. In: Zhang, Y.X., Cherniak, D.J. (Eds.), Diffusion in Minerals and Melts. Mineralogical Society of America, Virginia, pp. 269–309.
Liebske, C., Schmickler, B., Terasaki, H., Poe, B.T., Suzuki, A., Funakoshi, K., Ando, R., Rubie, D.C., 2005. Viscosity of peridotite liquid up to 13 GPa: Implications for magma ocean viscosities. Earth Planet. Sci. Lett. 240, 589–604.
Meade, C., Hemley, R.J., Mao, H.K., 1992. High-pressure X-ray diffraction of SiO_2 glass. Phys. Rev. Lett. 69, 1387–1390.
Murakami, M., Bass, J.D., 2010. Spectroscopic evidence for ultrahigh-pressure polymorphism in SiO_2 glass. Phys. Rev. Lett. 104, 025504.
Mysen, B.O., Virgo, D., Kushiro, I., 1981. The structure role of aluminum in silicate melts – a Raman spectroscopic study at 1 atmosphere. Am. Mineral. 66, 678–701.
Mysen, B.O., Virgo, D., Seifert, F.A., 1982. The structure of silicate melts: Implications for chemical and physical properties of natural magma. Rev. Geophys. Space Phys. 20, 353–383.
Phillips, J.C., 1979. Topology of covalent non-crystalline solids I: Short-range order in chalcogenide alloys. J. Non-Cryst. Solids 34, 153–181.
Plank, T., Langmuir, C.H., 1998. The chemical composition of subducting sediment and its consequences for the crust and mantle. Chem. Geol. 145, 324–394.
Poe, B.T., McMillan, P.F., Rubie, D.C., Chakraborty, S., Yarger, J., Diefenbacher, J., 1997. Silicon and oxygen self-diffusivities in silicate liquids measured to 15 gigapascals and 2800 kelvin. Science 276, 1245–1248.
Reid, J.E., Suzuki, A., Funakoshi, K., Terasaki, H., Poe, B.T., Rubie, D.C., Ohtani, E., 2003. The viscosity of $CaMgSi_2O_6$ liquid at pressures up to 13 GPa. Phys. Earth Planet. Inter. 139, 45–54.
Richet, P., Lejeune, A.-M., Holz, F., Roux, J., 1996. Water and the viscosity of andesite melts. Chem. Geol. 128, 185–197.
Riebling, E.F., 1966. Structure of sodium aluminosilicate melts containing at least 50 mole% SiO_2 at 1500 °C. J. Chem. Phys. 44, 2857–2865.
Rivers, M.L., Carmichael, I.S.E., 1987. Ultrasonic studies of silicate melts. J. Geophys. Res. 92, 9247–9270.
Sakamaki, T., Suzuki, A., Ohtani, E., Terasaki, H., Urakawa, S., Katayama, Y., Funakoshi, K., Wang, Y., Hernlund, J.W., Ballmer, M.D., 2013. Ponded melt at the boundary between the lithosphere and asthenosphere. Nat. Geosci. 6, 1041–1044.
Salmon, P.S., Martin, R.A., Mason, P.E., Cuello, G.J., 2005. Topological versus chemical ordering in network glasses at intermediate and extended length scales. Nature 435, 75–78.
Salmon, P.S., Barnes, A.C., Martin, R.A., Cuello, G.J., 2006. Glass fragility and atomic ordering on the intermediate and extended range. Phys. Rev. Lett. 96, 235502.
Salmon, P.S., Drewitt, J.W.E., Whittaker, D.A.J., Zeidler, A., Wezka, K., Bull, C.L., Tucker, M.G., Wilding, M.C., Guthrie, M., Marrocchelli, D., 2012. Density-driven structural transformations in network forming glasses: a high-pressure neutron diffraction study of GeO_2 glass up to 17.5 GPa. J. Phys. Condens. Matter 24, 415102.
Sanchez-Valle, C., Bass, J.D., 2010. Elastic and pressure-induced structural changes in vitreous $MgSiO_3$-enstatite to lower mantle pressures. Earth Planet. Sci. Lett. 295, 523–530.
Sato, T., Funamori, N., 2008. Sixfold-coordinated amorphous polymorph of SiO_2 under high pressure. Phys. Rev. Lett. 101, 255502.
Sato, T., Funamori, N., 2010. High-pressure structural transformation of SiO_2 glass up to 100 GPa. Phys. Rev. B 82, 184102.
Sugai, S., Onodera, A., 1996. Medium-range order in permanently densified SiO_2 and GeO_2 glass. Phys. Rev. Lett. 77, 4210–4213.
Susman, S., Volin, K.J., Price, D.L., Grimsditch, M., Rino, J.P., Kalia, R.K., Vashishta, P., 1991. Intermediate-range order in permanently densified vitreous SiO_2: A neutron-diffraction and molecular-dynamics study. Phys. Rev. B 43, 1194–1197.
Suzuki, A., Ohtani, E., Terasaki, H., Funakoshi, K., 2005. Viscosity of silicate melts in $CaMgSi_2O_6$–$NaAlSi_2O_6$ system at high pressure. Phys. Chem. Miner. 32, 140–145.
Suzuki, A., Ohtani, E., Terasaki, H., Nishida, K., Hayashi, H., Sakamaki, T., Shibazaki, Y., Kikegawa, T., 2011. Pressure and temperature dependence of the viscosity of a $NaAlSi_2O_6$ melt. Phys. Chem. Miner. 38, 59–64.
Taniguchi, H., 1992. Entropy dependence of viscosity and the glass-transition temperature of melts in the system diopside–anorthite. Contrib. Mineral. Petrol. 109, 295–303.
Thorpe, M.F., 1983. Continuous deformations in random networks. J. Non-Cryst. Solids 57, 355–370.
Tsiok, O.B., Brazhkin, V.V., Lyapin, A.G., Khvostantsev, L.G., 1998. Logarithmic kinetics of the amorphous–amorphous transformations in SiO_2 and GeO_2 glass under high pressure. Phys. Rev. Lett. 80, 999–1002.
Tsuchiya, T., 2003. First-principles prediction of the P–V–T equation of state of gold and the 660 km discontinuity in Earth's mantle. J. Geophys. Res. 108. http://dx.doi.org/10.1029/2003JB002446.
Wang, Y., Sakamaki, T., Skinner, L.B., Jing, Z., Yu, T., Kono, Y., Park, C., Shen, G., Rivers, M.L., Sutton, S.R., 2014. Atomistic insight into viscosity and density of silicate melts under pressure. Nat. Commun 5. http://dx.doi.org/10.1038/ncomms4241.
Wolf, G.H., McMillan, P.F., 1995. Pressure effects on silicate melt structure and properties. In: Stebbins, J.F., McMillan, P.F., Dingwell, D.B. (Eds.), Structure, Dynamics and Properties of Silicate Melts. Mineralogical Society of America, Virginia, pp. 505–562.
Xue, X., Stebbins, J.F., Kanzaki, M., Tronnes, R.G., 1989. Silicon coordination and speciation changes in a silicate liquid at high pressures. Science 245, 962–964.
Xue, X., Stebbins, J.F., Kanzaki, M., McMillan, P.F., Poe, B., 1991. Pressure-induced silicon coordination and tetrahedral structural changes in alkali silicate melts up to 12 GPa: NMR, Raman, and infrared spectroscopy. Am. Mineral. 76, 8–26.
Yamada, A., Wang, Y., Inoue, T., Yang, W., Park, C., Yu, T., Shen, G., 2011. High-pressure X-ray diffraction studies on the structure of liquid silicate using a Paris–Edinburgh type large volume press. Rev. Sci. Instrum. 82, 015103.
Yokoyama, A., Matsui, M., Higo, Y., Kono, Y., Irifune, T., Funakoshi, K., 2010. Elastic wave velocities of silica glass at high temperatures and high pressures. J. Appl. Phys. 107, 123530.
Zha, C.S., Hemley, R.J., Mao, H.-K., Duffy, T.S., Meade, C., 1994. Acoustic velocities and refractive index of SiO_2 glass to 57.5 GPa by Brillouin scattering. Phys. Rev. B 50 (18), 13105.